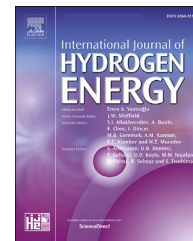




ELSEVIER

Available online at [www.sciencedirect.com](http://www.sciencedirect.com)

ScienceDirect

journal homepage: [www.elsevier.com/locate/he](http://www.elsevier.com/locate/he)

# Low-temperature Cu/Zn/SBA-16 integrating carbon membrane reactor for hydrogen production and high CO conversion through water-gas shift reaction

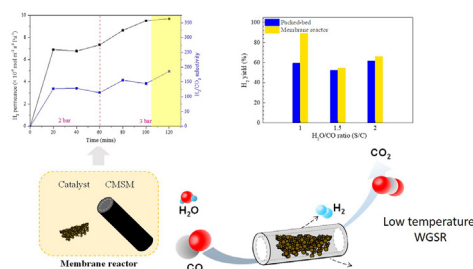
Jing-Yi Li, Ming-Yen Wey<sup>\*</sup>, Hui-Hsin Tseng<sup>\*\*</sup>

Department of Environmental Engineering, National Chung Hsing University, Taichung 402, Taiwan, ROC

## HIGHLIGHTS

- A tubular CMS membrane reactor was synthesized for the low temperature WGS reaction.
- CMS membrane shows excellent perm-selectivity toward H<sub>2</sub>/CO<sub>2</sub> of 185.64.
- The CO conversion of MR reaches 99% at 300 °C.
- Modification with a hydrophobic Si layer enhanced the CO conversion.
- The optimal hydrogen recovery of 100% was obtained at S/C = 2.

## GRAPHICAL ABSTRACT



## ARTICLE INFO

### Article history:

Received 22 March 2022

Received in revised form

9 November 2022

Accepted 18 November 2022

Available online xxx

### Keywords:

Carbon molecular sieve membrane

Membrane reactor

Water gas shift reaction

Hydrophobic modification

Gas separation

## ABSTRACT

The increasing demand for H<sub>2</sub> energy has led to a great amount of research being conducted in a membrane reactor (MR), in which a membrane is applied during the water-gas shift (WGS) reaction. In this study, Cu/Zn/SBA-16 WGS catalysts and carbon molecular sieve (CMS) membranes were integrated into CMS MRs. To improve the CO conversion and H<sub>2</sub> yield, C MRs were investigated, and different steam/CO (S/C) ratios were used to evaluate the conversion performance. In this study, a tubular CMS membrane was used as the membrane material for a MR. The as-prepared CMS membrane exhibited excellent selectivity of 185.64 for H<sub>2</sub> and CO<sub>2</sub> mixed gas, and an ideal H<sub>2</sub> permeability of  $9.7 \times 10^{-9} \text{ mol m}^{-2} \text{ s}^{-1} \text{ Pa}^{-1}$  when operated under low temperature/pressure conditions (300 °C/3 bar). The Cu/Zn/SBA-16 catalyst synthesized via coprecipitation was used in the WGS reaction. With a relatively low reaction temperature of 300 °C, 2500 h<sup>-1</sup> gas hourly space velocity, and S/C equal to 1.5, the CO conversion efficiency of MR could reach up to 99%, and the recovery of H<sub>2</sub> was approximately 76%. However, as the S/C increased to 2, the H<sub>2</sub> recovery increased to 99%, whereas the CO conversion decreased to 89% because of the water vapor adsorbed on the active site. The hydrophobic Si/C-modified membrane was

<sup>\*</sup> Corresponding author.

<sup>\*\*</sup> Corresponding author.

E-mail addresses: [mywey@dragon.nchu.edu.tw](mailto:mywey@dragon.nchu.edu.tw) (M.-Y. Wey), [hhtseng@nchu.edu.tw](mailto:hhtseng@nchu.edu.tw) (H.-H. Tseng).

<https://doi.org/10.1016/j.ijhydene.2022.11.199>

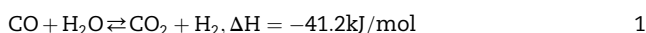
0360-3199/© 2022 Hydrogen Energy Publications LLC. Published by Elsevier Ltd. All rights reserved.

further synthesized and showed outstanding performance in CO conversion of over 99% with S/C equal to 2.

© 2022 Hydrogen Energy Publications LLC. Published by Elsevier Ltd. All rights reserved.

## Introduction

Integrated gasification combined cycle (IGCC) systems combine the gasification process and cycle power generation and have significant advantages, such as zero pollution, high efficiency, and diverse selectivity of feedstocks, which not only offers an inexpensive C capture and storage method but also provides H<sub>2</sub> production for utilization in other industrial and chemical processes [1,2]. The water-gas shift (WGS) reaction and gas separation system were designed to improve the H<sub>2</sub> yield and C capture in the IGCC system. The WGS reaction is a well-known mildly exothermic reaction that has been widely applied in industry for several years [3–5]. The basic WGS reaction is given in Eq. 1:



Low temperatures are favorable for increasing the amount of H<sub>2</sub> and the conversion of CO. Therefore, the WGS reaction is a two-step process for industrial applications [5,6]. The first reaction was performed at a high-temperature shift of 370–400 °C using Fe–Cr oxides as the catalyst, whereas the second reaction was operated at a low-temperature shift of 190–250 °C using Cu–Zn oxides as the catalyst [7,8]. The equilibrium coefficient of the WGS reaction decreases with increasing temperature; therefore, H<sub>2</sub> tends to be generated at low temperatures. Among the low-temperature WGS reaction catalysts, Cu-based catalysts are considered to have the highest potential [9–13]. To date, many different Cu-based catalysts have been reported to exhibit high activity in low-temperature reactions, such as Cu/Zn, Cu/ZnO/Al<sub>2</sub>O<sub>3</sub>, Cu–Mn spinel oxide, and Cu/CeO<sub>2</sub>, which have been commercialized as catalysts for low-temperature WGS reactions [9,14]. Most Cu/Zn WGS catalysts are prepared by the coprecipitation method for two reasons: (1) the coprecipitation method is a simple and economical method for preparation considering the large industrial demand; and (2) hydroxycarbonates are the best precursors during coprecipitation and have a higher active Cu surface area after treatment [15]. However, in previous studies, the specific surface area of the Cu/Zn catalyst has not been particularly prominent, and the redox mechanism of the active Cu phase has also been affected by the support, which changes the redox reaction temperature. Therefore, in terms of support, high efficiency of mass transfer and high specific area are the main considerations.

SBA-16 belongs to the SBA series in which pores in the structure are arranged in a cubic shape and spherical micropores are connected with smaller pores to form a multidirectional symmetrical structure. Therefore, both the pore diffusivity of the reactants and the catalytic interaction with the metal support are better in three-dimensional space than in two-dimensional space, and the mass transfer effect can be

improved [16]. According to Azizi et al. [17], SBA-16 has a thicker pore wall (5–8 nm), resulting in outstanding thermal stability, and a pore size of 5–15 nm, which can reduce the diffusion resistance of molecules in the catalyst, is considered to be the ideal catalyst support [18,19]. Moreover, the Si–OH functional group in SBA-16 facilitates the water vapor transfer reaction [20]. However, the use of SBA-16 as a support material is rare. Herein, the development of a Cu/Zn/SBA-16 catalyst was the focus. Membrane reactors (MRs) have been investigated because they increase H<sub>2</sub> yield and CO conversion and allow the simultaneous production and separation of products. These reactors combine the WGS reaction and the gas separation system into one process, thus, overcoming the thermodynamic limitations of the WGS reaction [4,6,21]. The concept of MRs can be traced back to the 1960s when membranes were used as active participants in chemical conversion by integrating the membrane and catalyst, which enhanced the reaction rate, selectivity, and yield. The membrane in a MR acts not only as a separator but also as a part of the reactor. MRs can continuously select and remove one or more products to increase the yield [22].

Currently, metal and porous inorganic membranes are used in pre-combustion C recovery procedures. Among the types of H<sub>2</sub>-selective membranes, metal Pd membranes or alloy-type membranes, such as Ni, Cu, and Fe, can generate H<sub>2</sub> with a purity higher than 99.99% [23,24]. Therefore, conventional H<sub>2</sub>-selective MR [25–27] includes polymer membranes [28], dense Pd membranes [26–30], and Ni and ceramic membranes [25,31–33]. Several studies have evaluated WGS reaction activity in different MRs using various catalysts [34]. For instance, tubular Pd-based membranes using Fe–Cr catalysts have been shown to achieve a CO conversion rate of 59 [35,36], a Pd–Ag hollow fiber membrane with CuO/CeO<sub>2</sub> achieved H<sub>2</sub> recovery of 28% and CO conversion of 51% [37], and a tubular Si membrane with a Cu/ZnO/Al<sub>2</sub>O<sub>3</sub> catalyst achieved H<sub>2</sub> recovery of 40–80% and a CO conversion of 80% [38]. Based on the results from the past few years, these studies have mainly focused on Si, Pd, and Pd-alloy membranes [39–41]. Because Pd has a unique ability of H<sub>2</sub> permselectivity, a very high H<sub>2</sub> permeability can be obtained at appropriate operating temperatures. However, Pd membranes have a short service life and need to be replaced within a few months. Therefore, the high operation and maintenance costs are potential problems that prevent Pd membranes from being used at a large scale. In addition, with low thermal stability, this type of membrane is easily destroyed during the thermal treatment cycle, the membrane is easily contaminated by sulfur [35,36] and H<sub>2</sub> transmission can be blocked by CO. Furthermore, metallic membranes are more expensive than other membranes, such as C, ceramic, and zeolite membranes, limiting their applications. For the reasons mentioned above, alternative materials, such as C molecular sieve (CMS) membranes and Si membranes, have become available and are promising

alternative MR materials [30,42,43]. C, ceramic, and zeolite membranes show higher thermal stability, chemical resistance, and environmental resistance, which seem to be more suitable for industrial applications. For this reason, alternative materials, such as CMS membranes and Si membranes, are available and will become the most promising alternative MR materials in the future [30,42,44].

To select an outstanding material as a membrane reactor for application in the WGS reaction, environmental durability, chemical stability, and separation efficiency are crucial conditions that need to be considered [38]. A tubular CMS membrane is expected to be the optimum solution as a result of the following considerable benefits: ideal  $H_2/CO_2$  permselectivity [39,45], well-defined pore size, high thermal stability [46], and strong chemical resistance [40,41,47,48]; moreover, a tubular configuration has the advantages of a high specific area, high axial and radial symmetry, and easy integration with the catalyst [49].

However, the widespread use of CMS membranes in membrane reactors is limited by two major drawbacks: ease of cracking and fracture, and aging by water adsorption. As CMS membranes are exposed to steam during the WGS reaction, the C–O functional groups on the C membrane surface adsorb  $H_2O$  molecules by chemisorption and further block the effective size of the ultra-micropores of the C membrane [50,51]. As a result, the gas diffusion flux and separation performance of the membrane declines, which is the so-called “aging phenomenon”. The addition of hydrophobic materials is a conventional method for enhancing the hydrophobicity of C membrane reactors by providing a water resistance layer to prolong the lifetime of the C membrane [50–52].

To the best of our knowledge, there have been very few studies on C membrane reactors applied to low-temperature WGS reactions. Therefore, the aim of this study was to prepare a high-mechanical strength and high-permselectivity C membrane integrating a Cu–Zn/SBA-16 catalyst to fabricate a C membrane reactor for the WGS reaction. To enhance the antiwater adsorption, a superhydrophobic Si protective layer was coated on the surface of the C selective layer to prevent aging. The results of this study are expected to provide promising developments of high value by contributing towards the overcoming of limitations of CMS membrane reactors.

## Experimental

### Preparation of the Cu/Zn/SBA-16 catalyst

First, SBA-16 supports were prepared via hydrothermal synthesis [53,54]. The poly(alkylene oxide) triblock Pluronic F127 (Sigma Aldrich Chemical Co. USA) was mixed with 2 M HCl. Then, TEOS (Si precursor; Fluka, Germany) was added and the mixture was stirred at 40 °C for 3 h. The resulting gel was then hydrothermally treated at 110 °C in an oven. The solid product was then filtered, rinsed using a centrifuge, and then dried overnight at 110 °C. Finally, it was calcined at 500 °C for 6 h to remove the templates. The Cu/Zn/SBA-16 catalyst used in this study was fabricated using a coprecipitation method. The molar ratio of Cu:Zn:Si was 3:3:1 (XPS and EDS analyses confirmed the proportion of elements and are shown in Figs.

S8 and S9 and Table S2). SBA-16 particles were dispersed in appropriate DI water first and stirred at 65 °C to form a homogeneous suspension.  $Cu(NO_3)_2 \cdot 6H_2O$  (purity 100%, J.T. Baker Co. USA) and  $Zn(NO_3)_2 \cdot 6H_2O$  (purity 100%, J.T. Baker Co. USA) were added to the DI water and were then stirred at 65 °C to prepare 6 M metal precursor solution.  $Na_2CO_3$  (purity 99.81%, Choneye) with appropriate DI water was stirred at 65 °C to form 1.6 M precipitant. Finally, the metal precursor solution and precipitant mentioned were added dropwise into SBA-16 suspending solution, and the solution pH was 6.5–7 and the temperature was maintained at 65 °C. Then, the resulting solution was left for 1 h at 65 °C and filtered, then dried overnight at 110 °C. Finally, the resulting product was calcined at 350 °C for 3 h at a 5 °C/min ramping rate.

### Preparation of tubular CMS membranes

Here, as reported in our previous work [55,56], tubular CMS membranes were obtained by dip-coating and carbonization of a polyetherimide (PEI) precursor (the chemical structure of the PEI polymer precursor is shown in Fig. S4). Tubular substrates with a length of 5 cm, an external diameter of 1.2 cm, and an internal diameter of 0.8 cm were supplied by the Yuen Jinn Electrical Ceramic Co., Ltd. (Taiwan). The 10 wt% polymer solution was prepared by dissolving PEI precursors with a repeating unit of 592 g/mol (Sigma Aldrich Chemical Co. USA) in N-methylpyrrolidone (Mallinckrodt Chemicals Co., USA) and stirring for 24 h. Then, the polymer solution was dip-coated in the Ti/Al<sub>2</sub>O<sub>3</sub> modified tubular substrate with a 1 mm/s rate of immersion and withdrawal assisted by a vacuum pump for 20 s to form polymer membranes [55]. The as-prepared polymer membranes were then carbonized at 700 °C for 2 h at a 5 °C/min heating rate after drying overnight at approximately 30 °C.

### Hydrophobic modification of the CMS membrane

The trichlorododecylsilane (purity ≥95.0%, Sigma Aldrich Co. USA.) was used directly as hydrophobic material for carbon membrane surface modification without any pretreatment or dilution. The hydrophobic layer was coated via dip-coating method for 1-min retention and then was placed in oven at 60 °C for 30 min to evaporate superfluous solvent.

### Characterization

The surface micrograph of membranes and catalysts were observed by field-emission scanning electron microscopy (FE-SEM; model: JEOL JSM-6700F) equipped with EDS.

The crystalline structure and d-spacing of catalysts were analyzed by X-ray diffraction (XRD; model: BRUKER D8 SSS) with a Cu–K $\alpha$  radiation source ( $\lambda = 1.542 \text{ \AA}$ ). The diffraction intensities were examined at 2 $\theta$  angle ranges between 10° and 80° with a 2°/min scanning rate.

The specific surface area and porous properties were performed by N<sub>2</sub> sorption method at –196 °C and calculated using Barrett–Johner–Halenda (BJH) method by Brunauer–Emmett–Teller (BET; model: ASAP2010). Before the analysis, all the samples needed to be heated under 110 °C over 10 h to remove water vapor and impurities.

The dynamic analysis of contact angle of membrane was examined using a contact angle meter (CA; model: KRÜSS DSA100). The program recorded the average angles on the left and right of the liquid drop on the surface of membrane. Each sample was measured for 3 points, which was measured and averaged by total of 5 s, then repeated the experiment mentioned above three times.

The transmission morphology of the catalysts was observed by transmission electron microscopy (TEM; model: JEM 1400 JEOL, 120 keV).

Hydrogen temperature-programmed reduction ( $H_2$ -TPR) with a thermal conductivity detector (TCD) was employed to determine the reduction behavior of the catalysts. Prior to  $H_2$  reduction, 0.2 g catalyst was pretreated at 200 °C under Ar gas flow (20 mL/min) for an hour. Afterward, the reduction in the temperature in the range of 100 °C–500 °C was recorded in the 5%  $H_2$ /Ar (30 mL/min) gas flow at a ramping rate of 10 °C/min.

The chemical state and elemental composition of the resultant catalysts and membranes were detected by X-ray photoelectron spectroscopy (XPS) equipped with Al-K $\alpha$  radiation (PHI 5000 Versa Probe, MN, USA).

The particle size distribution of the synthesized SBA-16 was analyzed by dynamic light scattering spectroscopy (DLS; model: nano SAQLA). The SBA-16 powder needs to be fairly uniformly suspended in water and repeatedly sonicated prior to analysis to ensure good dispersion.

#### Permeation studies of the CMS membranes

A single gas permeation test was performed to examine the performance of the tubular CMS membranes, which used the constant volume/variable pressure method with a lab-made facility, as shown schematically in Fig. 1. The membranes were first placed in a stainless-steel cell, and both closed ends of the tubes were then sealed with rubber O-rings to avoid

leakage. Subsequently, both the upstream and downstream sides of the system were degassed at ambient temperature to ensure no disturbance. Subsequently, pure gas ( $H_2$ ,  $CO_2$ ,  $O_2$ ,  $N_2$ , and  $CO$ ) was fed into the feed side individually in an inside-out flow pattern. The permeability of pure gas was measured at a feed pressure of 2 bar. Gas permeability and ideal gas selectivity were calculated using the following equations: where  $dp/dt$  is the slope (cm-Hg/s) of the pressure that varies with time in the pseudo-steady state;  $V$  is the downstream volume ( $cm^3$ ) of gas permeation;  $\Delta p$  (cm-Hg) is the difference in pressure between the two sides of the membrane;  $A$  is the effective membrane area ( $cm^2$ );  $L$  is the membrane thickness (cm);  $P_0$  is 76 cm Hg;  $T_0$  is 273 K; and  $T$  is the measured temperature (K) at 298 K.

$$\alpha_{A/B} = \frac{P_A}{P_B} \quad (2)$$

where  $\alpha_{A/B}$  is the ideal selectivity coefficient of gas A and B, which is reported as the ratio of the permeability of A and B ( $P_A$  and  $P_B$ ).

#### Catalytic activity measurements

Catalytic activity tests in the WGS reaction were carried out individually on packed-bed and C membrane reactors. In the catalytic activity measurements of the membrane reactor, as shown schematically in Fig. 1 (position 7), the catalyst was uniformly dispersed in a quartz wool sheet, rolled into a cylindrical shape, and inserted into the tubular CMS membrane. The actual products are illustrated in Fig. S1. The flow pattern of the syngas was inside-out, and the simulated syngas containing  $H_2$ ,  $CO$ ,  $CO_2$ , and  $N_2$  was mixed before being fed into the membrane reactor (the composition is shown in Table 1). Prior to the catalytic reaction, reduction was carried out at 300 °C for 2 h at a total flow rate of 100 mL/min of 20%  $H_2/N_2$ .

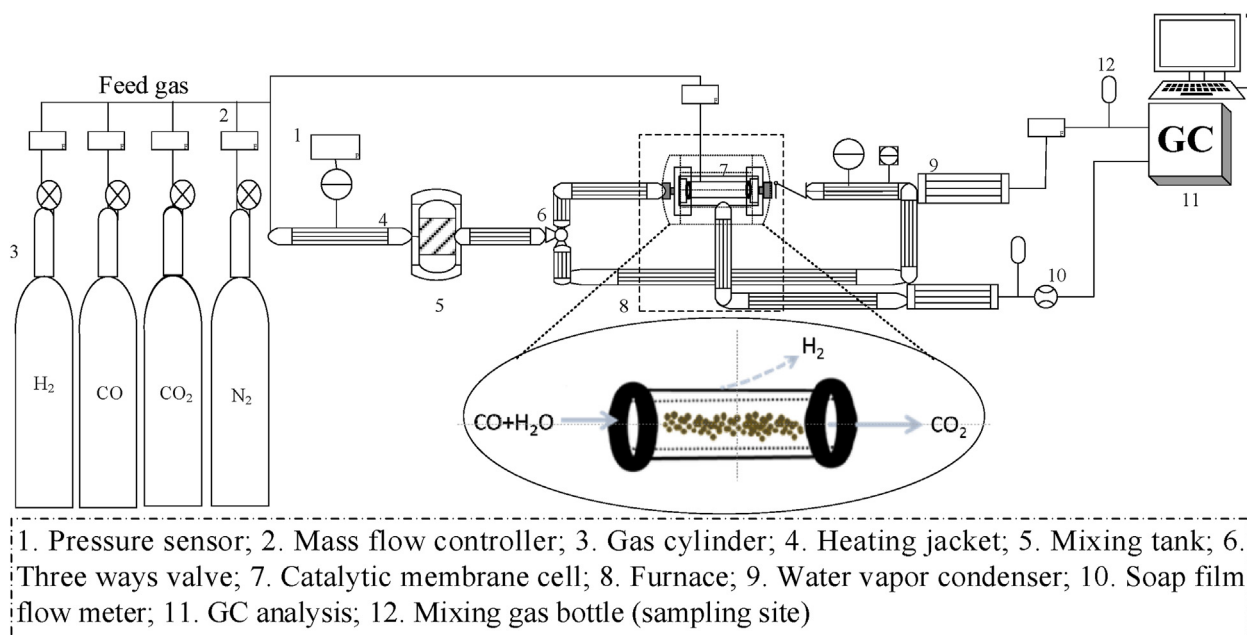


Fig. 1 – Schematic of the C membrane reactor equipment (self-assembled equipment).

**Table 1 – Conditions of the catalytic reaction.**

Item	Condition
Catalyst	Cu/Zn/SBA-16
Flow rate (ml/min)	50
Feed gas composition (vol%, dry basis)	CO 40%, H <sub>2</sub> 30%, CO <sub>2</sub> 10%, N <sub>2</sub> 20%
H <sub>2</sub> O/CO (S/C)	1, 1.5, 2
Pressure (kg/cm <sup>2</sup> )	3
Reaction temperature (°C)	200, 250, 300
Space velocity (h <sup>-1</sup> )	2,500, 5,000, 10,000

Quantitative water was also fed into the mixing tank (position no. 5) where gases would go through and accumulate pressure to ensure that the gases and water vapor produced by evaporation with thermal heating were homogeneously mixed. After the complete reaction between the feed gas and the catalyst, H<sub>2</sub> on the permeation side was separated through the membrane, and CO<sub>2</sub> on the concentration side was released.

Prior to conducting a series of activity tests, repeated experiments were conducted to ensure the quality and reliability of the experimental data in the early stages of the experiment, as shown in Fig. S2.

Subsequently, the gas compositions of the upstream and downstream sides of the system were measured. During the reaction, sweep gas (N<sub>2</sub>) was used to promote the removal of H<sub>2</sub>. The outlet stream was estimated by taking a sample every 30 min with a needle and then injecting it into a gas chromatograph (GC) for analysis. The GC (Clarus 500 GC, PerkinElmer) with a Carboxen 1000 column equipped with a thermal conductivity detector was used to determine the concentrations of H<sub>2</sub>, CO, N<sub>2</sub>, and CO<sub>2</sub>.

The H<sub>2</sub> gas permeability ( $P_{H_2}$ ), H<sub>2</sub> recovery ( $R_{H_2}$ ) and CO conversion ( $X_{CO}$ ) were calculated using equations as following:

$$Q_i = \frac{X_i \cdot Q}{A} \quad (3)$$

where  $Q_i$  represents the flux (ml/s),  $X_i$  denotes the volume concentration of gas, estimated by GC calibration curve,  $Q$  ((STP) ml/s) represents the total volume flow rate of permeate side, and  $A$  is the effective membrane area (cm<sup>2</sup>).

$$P_g = \frac{Q_i \cdot L}{\Delta p_i} \quad (4)$$

where  $P_g$  represents gas permeability (mol m<sup>-2</sup> s<sup>-1</sup> Pa<sup>-1</sup>),  $L$  is the membrane thickness (cm), where  $\Delta p_i$  (cmHg) represents the trans-membrane partial pressure drop for a specific gas.

$$R_{H_2} = \frac{[H_{2\text{sweep out}}]}{[H_{2\text{sweep out}}] + [H_{2\text{feed out}}]} \quad (5)$$

where  $R_{H_2}$  represents hydrogen recovery efficiency,  $H_{2\text{sweep out}}$  is the molar flow rate (mol/s) of H<sub>2</sub> of penetration, and the  $H_{2\text{feed out}}$  is the molar flow rate (mol/s) of H<sub>2</sub> of concentration.

$$X_{CO} = \frac{[CO_{\text{feed in}}] - [CO_{\text{feed out}}] - [CO_{\text{sweep out}}]}{[CO_{\text{feed in}}]} \quad (6)$$

where  $X_{CO}$  represents CO conversion efficiency,  $CO_{\text{feed in}}$  is the molar flow rate (mol/s) of CO of feed stream; the  $CO_{\text{feed out}}$  is the molar flow rate (mol/s) of CO of concentration side, and the

$CO_{\text{sweep out}}$  is the molar flow rate (mol/s) of CO of the penetration side.

## Results and discussion

### Characterization of WGS catalysts

#### Crystallinity analysis

The small-angle X-ray diffraction (XRD) pattern of the SBA-16 supports is shown in Fig. 2 (a). The strong peaks exhibited at 0.77° (110), 1.09° (200), and 1.34° (211) individually indicate the three-dimensional cubic  $Im3m$  symmetry structure of SBA-16 [54] (see Fig. S3). Fig. 2 (b) shows the diffraction pattern of the Cu/Zn/SBA-16 catalyst before calcination (black line) and after calcination (red line) using an XRD instrument. The results showed that the non-calcined Cu/Zn/SBA-16 catalyst was mainly composed of aurichalcite ((Cu<sub>1-x</sub>Zn<sub>x</sub>)<sub>5</sub>(OH)<sub>6</sub>(CO<sub>3</sub>)<sub>2</sub>, ICDD17-0743), with main characteristic peaks of 13.7° (200), and malachite (Cu<sub>2</sub>CO<sub>3</sub>(OH)<sub>2</sub>, ICDD 41-1390). The crystal phase of the calcined catalyst was converted to black Cu (tenorite: CuO; ICDD 48-1548) and zincite (ZnO; ICDD 36-1451), which are mainly composed of CuO and ZnO, with the main characteristic peaks being 35.6° (111) and 31.8° (110), respectively [57,58]. Nakamura et al. [59] used Zn to deposit a single Cu crystal for the synthesis of methanol with CO<sub>2</sub>. They proposed that the reaction was accelerated when Zn was deposited on CuO (111); however, the reaction was delayed when Zn was deposited on CuO (110) and CuO (100). Moreover, the selectivity and activity of the derived catalysts were better when the as-prepared Cu/ZnO catalysts contained aurichalcite in their precursor, which could be attributed to the Cu atoms being segregated by Zn atoms and transformed into highly dispersed CuO particles with smaller particle sizes after calcination [60]. Conversely, for malachite, the composition structure is not assisted by Zn atoms; therefore, it may be transformed into Cu with low dispersion and larger particle size after calcination. Therefore, the WGS catalysts prepared in this study show that the catalyst precursor containing aurichalcite is expected to possess higher catalyst selectivity and activity. In the process of H<sub>2</sub> production, the catalysts can not only decrease the reaction temperature, increase the concentration of the expected product, and improve the conversion of the reactant, but can also be expected to have a longer service life, allowing the reaction to proceed without decay. Since the main reaction site for the low-temperature WGS reaction is metallic Cu, the higher Cu content in the catalyst can promote the increase of active sites at the interface of CuO and the metal oxide, thereby improving the catalytic performance. Fig. S7 shows the H<sub>2</sub>-TPR characterization to prove CuO formation and investigate the H<sub>2</sub> reducibility properties of the Cu/Zn/SBA-16 catalysts.

The above requirements for catalysts can be further understood through the catalytic reaction mechanism. There are two generally accepted reaction mechanisms of the WGS reaction, which can be summarized as the following reaction pathways [61–63]: the WGS reaction on the surfaces of metal oxides proceeds through (1) a reduction/oxidation mechanism

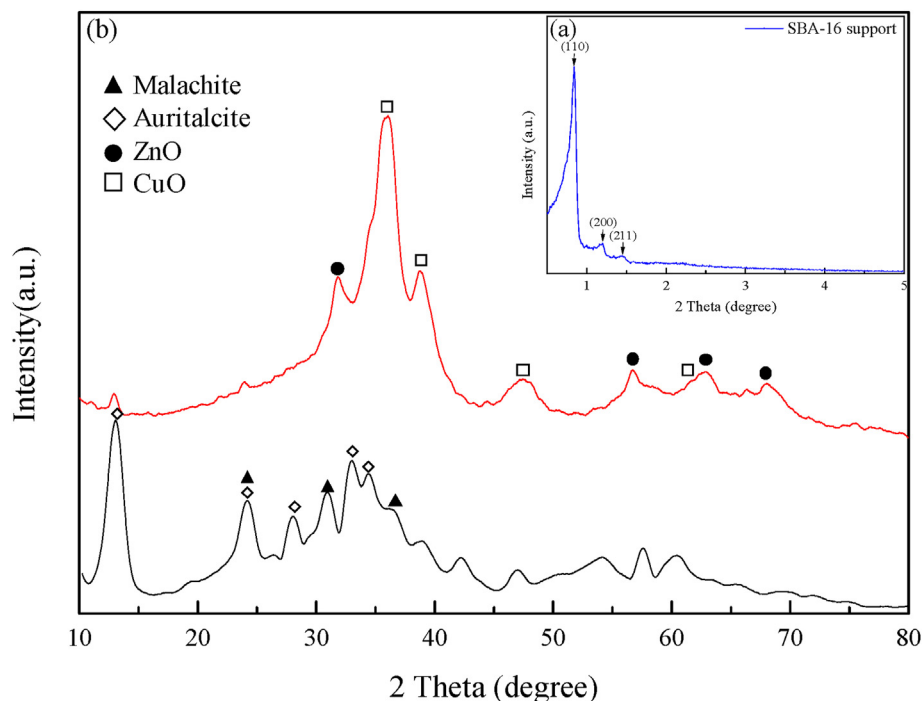


**Fig. 2 – XRD patterns of (a) SBA-16 support and (b) Cu/Zn/SBA-16 catalysts before and after calcination (non-calcined catalyst: black line; calcined catalyst: red line). (For interpretation of the references to color/colour in this figure legend, the reader is referred to the Web version of this article.)**

(see Fig. S6 (a)) and (2) a regenerative redox association mechanism (see Fig. S6 (b)). For the redox mechanism, the reaction steps and chemical reaction equations (see Equations (7) and (8) [64,65]) are as follows: (1) CO is adsorbed on the metal surface and reacts with O<sub>2</sub> supported on the surface; (2) after the reaction, CO<sub>2</sub> is generated, and the oxidative support is reduced simultaneously, resulting in the formation of O<sub>2</sub> vacancies on the support; and (3) through the dissociation of H<sub>2</sub>O, the reduced support is oxidized to generate H<sub>2</sub>. This repeated cycle can result in a complete WGS reaction.



The association mechanism of regenerative redox, also known as the hydroxyl pathway, is mainly carried out through the hydroxyl groups on the surface of the support: (1) CO adsorbs on the metal surface; (2) CO reacts with the OH group on the support surface to form a carboxyl or formic acid intermediate, which further dissociates to generate CO<sub>2</sub> and H<sub>2</sub>, forming an O<sub>2</sub> vacancy on the support; (3) the position of the O<sub>2</sub> vacancy on the support reacts with H<sub>2</sub>O; and (4) hydroxyl groups are generated.

#### Surface morphology and BET analysis of catalysts

Fig. 3 shows the FE-SEM images of the (a1) SBA-16 support and (a2) Cu/Zn/SBA-16 catalysts at 10,000× and 100,000× magnification. The SBA-16 supports synthesized by the hydrothermal synthesis method with a spherical appearance and microstructure on the surface can be observed in

graphs (a1) and (a2). However, as shown in Fig. 3 (a1), it was inferred that the active phase was deposited on the surface of the SBA-16 supports because after the active phase Cu and Zn were coated on the surface of SBA-16 with the coprecipitation method, and the surface of the catalyst presented villi-type. The magnification was then increased to 100,000× as shown in Fig. 3 (a2), where the microstructure of the villi was observed and it was found that a number of particles were actually stacked from the plate-like structure [66].

According to the classification of IUPAC [67], the adsorption and desorption curve of the SBA-16 support is defined as Type IV isotherm, indicating that the pore of the SBA-16 supports are mainly mesopores as shown in Fig. 3 (b1). In addition, the adsorption and desorption curve of Cu/Zn/SBA-16 shows the Type IV isotherm (Fig. 3 (b2)). Table 2 shows the specific surface area, average pore size, and pore volume of the SBA-16 supports and Cu/Zn/SBA-16 catalyst after BET analysis calculated by the BJH equation. The results show that the SBA-16 supports had a high specific surface area, its pore type distribution was dominated by mesopores and micropores, and its average pore size was 50.18 Å, which belonged to the mesopore structure. The specific surface area of the Cu/Zn/SBA-16 catalyst decreased from 611.34 to 81.18 m<sup>2</sup>/g compared with that of SBA-16 after coating of active phase Cu and Zn. The total pore volume also decreased from 0.7669 to 0.3329 cm<sup>3</sup>/g. However, the average pore size increased from 50.18 to 164.01 Å, and the distribution of the pore type was also changed from micropores and mesoporous-dominated structures to mesoporous and macromolecule-dominated structures. It was presumed that when the active phase metal was deposited on the supports, a portion of the active phase was inserted into its

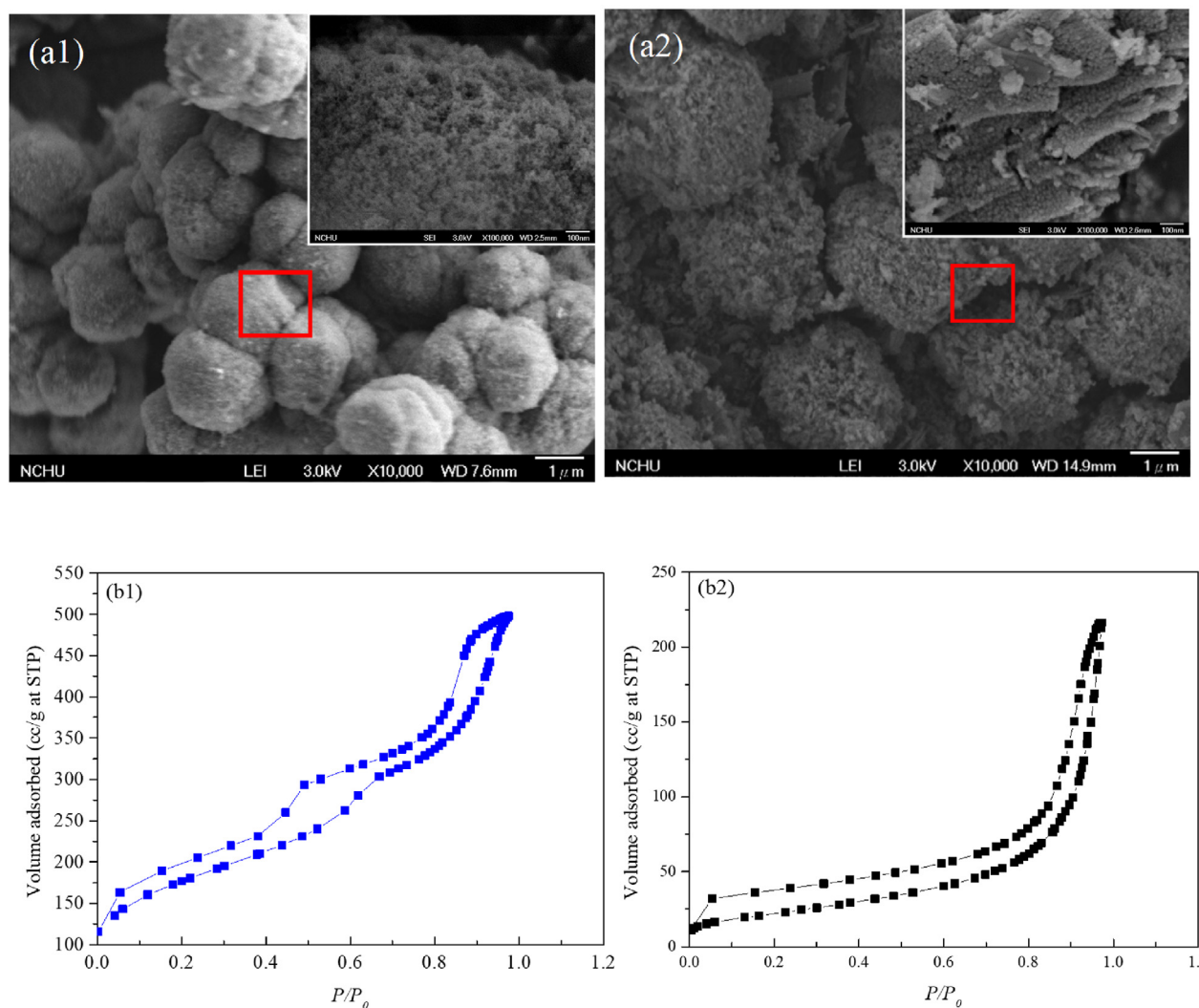


Fig. 3 – (a) FE-SEM images and (b)  $N_2$  adsorption-desorption isotherm of SBA-16 support and (2) Cu/Zn/SBA-16 catalysts.

Table 2 – Pore structure and characteristics of the support and catalyst.

Sample code	$S_{BET}$ ( $m^2/g$ )	$D_{pore}$ ( $\text{\AA}$ )	$V_{total}$ ( $cm^3/g$ )	$V_{micro}$	$V_{meso}$ ( $cm^3/g$ )	$V_{macro}$
SBA-16	611.34	50.18	0.7669	0.2579 (33.63%)	0.4889 (63.75%)	0.0201 (2.62%)
Cu/Zn/SBA-16	81.18	164.01	0.3329	0.0313 (9.4%)	0.2444 (73.42%)	0.0572 (17.18%)

micropores, resulting in a reduction in the proportion of microvoids, and a portion of the active phase was deposited on the surface of the supports, as shown in Fig. 3 (a2).

### Catalytic reaction of packed-bed

#### Effect of the reaction temperature

Before the test of the C membrane reactor commenced, the basic operating conditions, such as temperature, space velocity, and steam ratio, were evaluated with a packed bed to facilitate the operation of the C membrane reactor after obtaining the optimal conditions. Fig. 4 shows the CO conversion of the packed-bed reactor as a function of the reaction temperature. The results show that CO conversion increases significantly with increasing temperature. At

300 °C, the CO conversion reached approximately 82%, which was close to the equilibrium conversion. These results indicate that the operating temperature is a key factor controlling the reaction, and 300 °C is the optimal reaction environment. Although the WGS reaction is a weakly exothermic reaction, a relatively high operating temperature is still beneficial for obtaining high CO conversion. Compared to other studies [68], the Cu/Zn/SBA-16 catalysts selected could achieve a CO conversion of more than 80% at relatively low temperatures, which also confirmed the excellent catalytic performance of this catalyst.

#### Effect of space velocity

Based on packed-bed experiments, the effect of gas hourly space velocity (GHSV) on the WGS performance was also

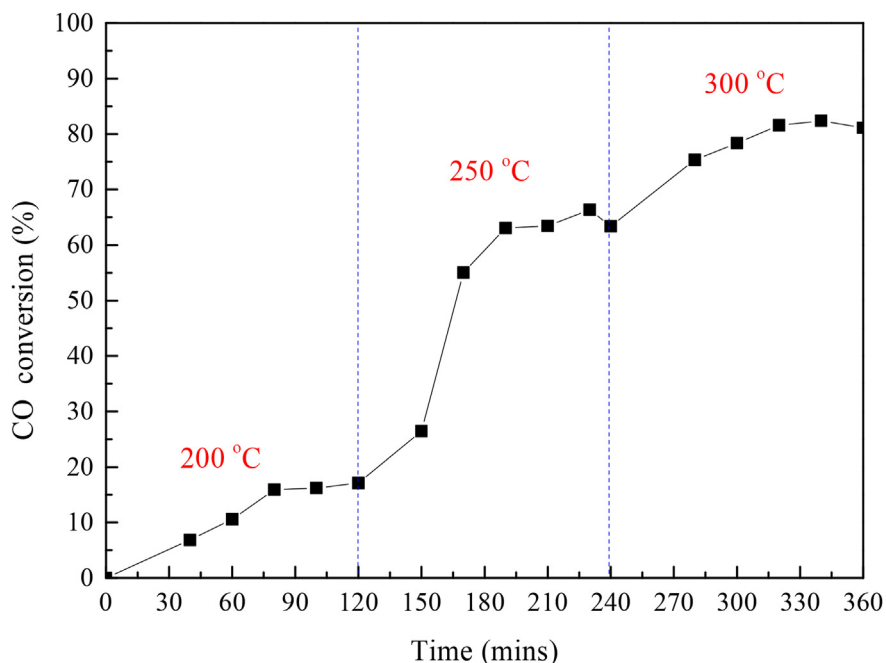


**Fig. 4** – LT-WGS activities of packed-bed reactor mode of Cu/Zn/SBA-16 catalysts as a function of reaction temperature. (reaction conditions: space velocity of 2500 h<sup>-1</sup>; S/C of 1).

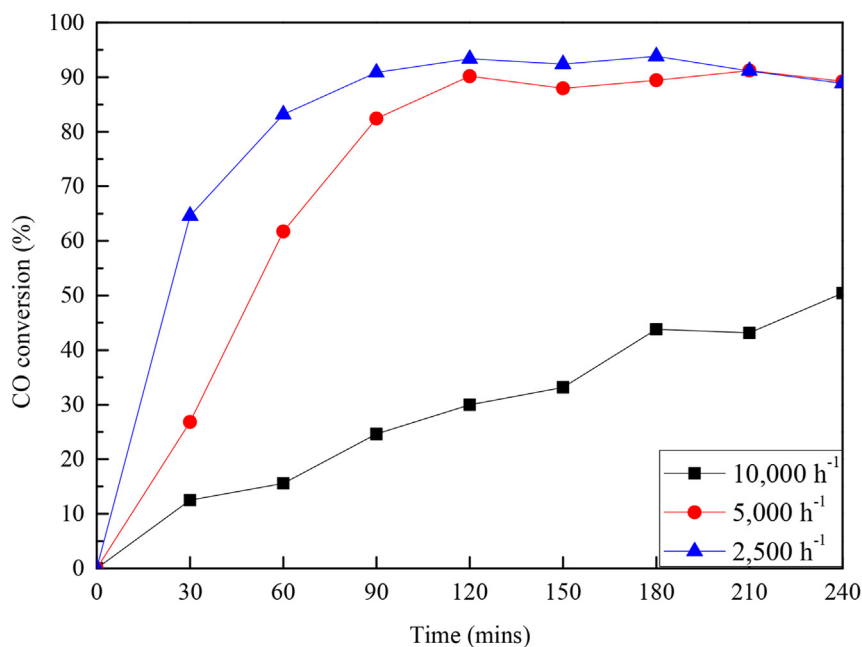


**Fig. 5** – LT-WGS activities of packed-bed reactor mode of Cu/Zn/SBA-16 catalyst as a function of space velocity. (reaction conditions: reaction temperature of 300 °C; S/C of 1).

investigated. Fig. 5 shows the CO conversion of the packed-bed reactor as a function of the GHSV. The results show that the CO conversion had a significant decreasing trend with an increase in GHSV. When the GHSV was 2500 h<sup>-1</sup>, the CO conversion was 93.82% at 300 °C and reached the equilibrium state. This result suggests that a lower GHSV increases the

residence time of the WGS reaction and provides sufficient reaction time for the reaction on the catalyst to convert CO, resulting in improved CO conversion. Therefore, we can expect CMS membrane reactors to have the opportunity to convert more CO at this low GHSV because membrane reactors are not limited by reactant accumulation problems.

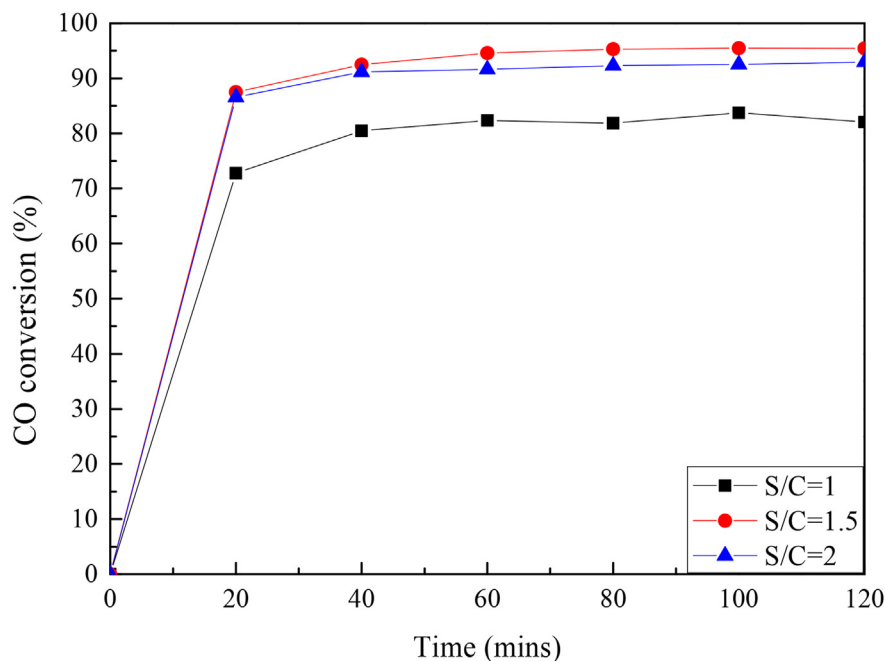


**Fig. 6 – LT-WGS activities of packed-bed reactor mode of Cu/Zn/SBA-16 catalyst as a function of H<sub>2</sub>O/CO ratio (S/C). (reaction conditions: reaction temperature of 300 °C; space velocity of 2500 h<sup>-1</sup>).**

#### Effect of the steam/CO ratio

Based on the packed-bed experiments, the CO conversion of the packed-bed reactor as a function of the steam/CO ratio (S/C) on the WGS performance is shown in Fig. 6. The CO conversion increases with increasing S/C ratio. When the S/C ratio was 1.0, the CO conversion reached 83.74%, and the improvement in CO conversion was even more pronounced at a S/C ratio of 1.5. However, a further increase in S/C resulted in a relative decrease in CO conversion. In general, the overall catalytic activity trend of the catalyst was that the steam ratio was proportional to the CO concentration of the retentate [41]. With a higher steam ratio, more H<sub>2</sub>O reactants could be provided, and the CO conversion of the catalytic activity could also increase [41]. However, the results of the reaction showed that the packed-bed reactor used in this study was accompanied by a decrease in the steam ratio, which was not consistent with the expected results. Therefore, the effect of S/C on the C membrane reactors was an important assessment for further discussion of membrane reactor performance.

#### Catalytic reaction and separation performance of the C membrane reactor

The permselectivity of the CMS membrane in terms of long-term stability and permeation performance is shown in Fig. 7. With increasing pressure, the permeability increased, while the H<sub>2</sub>/CO<sub>2</sub> selectivity also showed an increasing trend. The mixed gas separation performance of the CMS membrane at a pressure of 2 bar exhibited an excellent separation effect. The permeability of H<sub>2</sub> was  $6.78 \times 10^{-9} \text{ mol m}^{-2} \text{ s}^{-1} \text{ Pa}^{-1}$ , while the H<sub>2</sub>/CO<sub>2</sub> selectivity was 128.36, and this performance could

be maintained for 60 min. After pressurization, the permeability of H<sub>2</sub> increased to  $9.7 \times 10^{-9} \text{ mol m}^{-2} \text{ s}^{-1} \text{ Pa}^{-1}$ , and the H<sub>2</sub>/CO<sub>2</sub> selectivity was also greatly increased to 185.64, which showed that the as-prepared CMS membrane had excellent gas separation ability and could provide better H<sub>2</sub>/CO<sub>2</sub> selectivity at 3 bar.

Fig. 8 shows the permselectivity of the CMS membrane in the LT-WGS activities of the C membrane reactor mode of the Cu/Zn/SBA-16 catalyst as a function of the S/C ratio. According to the above test results of membrane separation ability, the best separation performance towards H<sub>2</sub>/CO<sub>2</sub> could be obtained at 3 bar, and the optimal catalytic reaction conditions were a reaction temperature of 300 °C and space velocity of

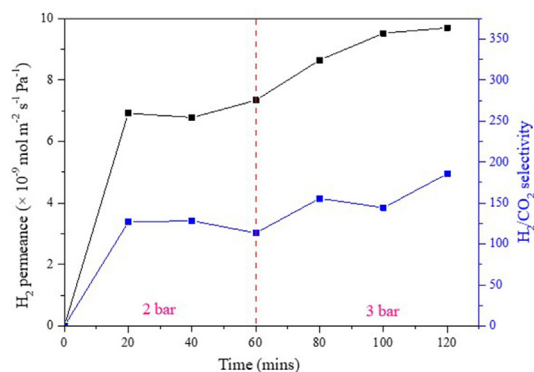


**Fig. 7 – The perm-selectivity of CMS membrane in long-term stability and permeation performance of membrane (operation conditions: temperature of 300 °C; different pressure: 2 and 3 bar).**

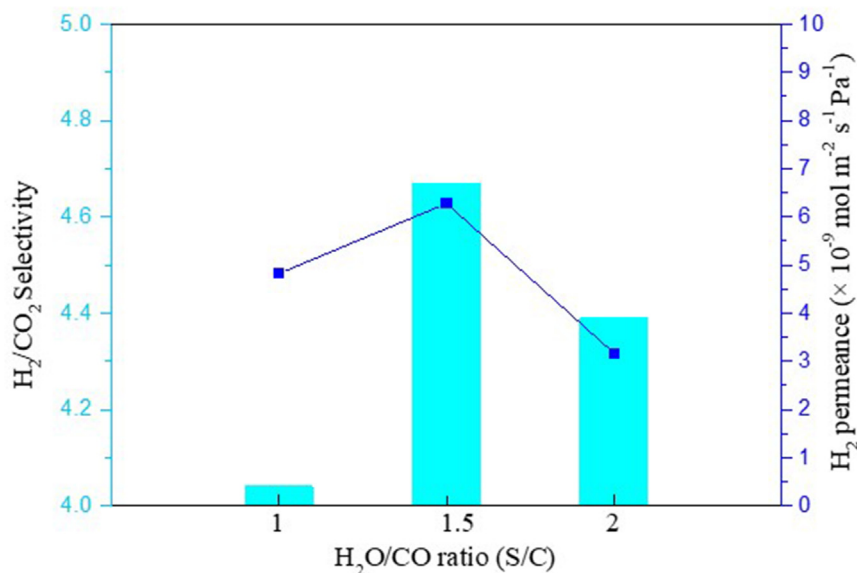


**Fig. 8** – The perm-selectivity of CMS membrane in LT-WGS activities of C membrane reactor mode of Cu/Zn/SBA-16 catalyst as a function of H<sub>2</sub>O/CO ratio (reaction conditions: reaction temperature of 300 °C; space velocity of 2500 h<sup>-1</sup>).

2500 h<sup>-1</sup>. The figure shows that when the S/C ratio is increased to 1.5, the selectivity and permeability of the CMS membrane will increase accordingly from 4.04 to 4.67 and 4.82 to 6.28 ( $\times 10^{-9} \text{ mol m}^{-2} \text{ s}^{-1} \text{ Pa}^{-1}$ ), respectively, but when the S/C ratio is increased to 2, the permselectivity of the membrane will be disabled, which may be because the active site of CO will be occupied, which will lead to a decrease in CO conversion, thereby reducing the permeability of H<sub>2</sub>. In addition, from the above experiments, it was found that the separation ability and permeability of the CMS membrane decreased significantly in a water-rich environment.

Fig. 9 shows a comprehensive comparison of the catalytic reaction results of packed-bed and C membrane reactors under different steam ratio conditions (S/C = 1, 1.5, and 2, respectively), and the reaction temperature was 300 °C. Fig. 9 (a) shows the CO conversion, Fig. 9 (b) shows the H<sub>2</sub> yield, and Fig. 9 (c) shows the H<sub>2</sub> recovery.

Compared to the results of the packed-bed reaction test, as shown in Fig. 9 (a1), when S/C = 1, X<sub>CO</sub> was 83.75%; when S/C = 1.5, X<sub>CO</sub> was up to 95.43%; and when S/C = 2, X<sub>CO</sub> was 92.95%. For the C membrane reactor catalytic performance shown in Fig. 9 (a2), when S/C = 1, X<sub>CO</sub> was 75.75%; when S/C = 1.5, X<sub>CO</sub> was 90% and even up to 100%; and, when S/C = 2, X<sub>CO</sub> was reduced to 89.36%. Overall, the C membrane reactor presented a better CO conversion rate (up to 100%), as the H<sub>2</sub> recovery also showed a high performance of up to 100%. Fig. 9 (b) presents a H<sub>2</sub> yield comparison between the packed-bed and C membrane reactor. As per the results shown in Fig. 9 (b), a C membrane reactor H<sub>2</sub> yield of 89.13% and packed-bed H<sub>2</sub> yield of 59.40% were obtained by S/C = 1, and a C membrane reactor H<sub>2</sub> yield of 54.69% and packed-bed H<sub>2</sub> yield of 52.54% were obtained at S/C = 1.5, while a C membrane

reactor H<sub>2</sub> yield of 66.32% and packed-bed H<sub>2</sub> yield of 61.78% were obtained at S/C = 2. The above results prove that the H<sub>2</sub> yield of the CMS membrane reactor under different steam ratios is slightly higher than that of the packed bed. As the S/C ratio increased, the CO conversion increased, whereas the H<sub>2</sub> yield showed the opposite trend. To the best of our knowledge, excessive steam may reduce the partial pressure of H<sub>2</sub> on the reaction side, resulting in low H<sub>2</sub> permeability and low H<sub>2</sub> yield, which is consistent with previous results of membrane permeation under different steam ratios. That is, when the CO conversion is higher, it compresses the H<sub>2</sub> yield and vice versa.

Fig. 9 (c) shows the H<sub>2</sub> recovery of the C membrane reactor. It was shown that the membrane reactor H<sub>2</sub> recovery was only 50–70% at S/C = 1 and 1.5, respectively, while when the steam ratio increased to S/C = 2, the H<sub>2</sub> recovery could be controlled at 80% or more, up to 100%. The H<sub>2</sub> recovery represents the molar ratio of the total amount of H<sub>2</sub> in the system to the H<sub>2</sub> content that penetrated the membrane, which is an important index for the performance evaluation of the membrane reactor [69]. The results showed that the H<sub>2</sub> recovery rate increased with an increase in the steam ratio. However, the stability of C membrane reactors requires further evaluation.

As is well known, the overall catalytic activity of catalysts is inversely proportional to the CO concentration of the retentate [70]. With a higher steam ratio, more H<sub>2</sub>O reactants can be provided, and the CO conversion of the catalytic activity also increases, thereby reducing the CO concentration of the outlet [70]. However, the results of the reaction here showed that the C membrane reactor used in this study was accompanied by a decrease in the steam ratio, which is not

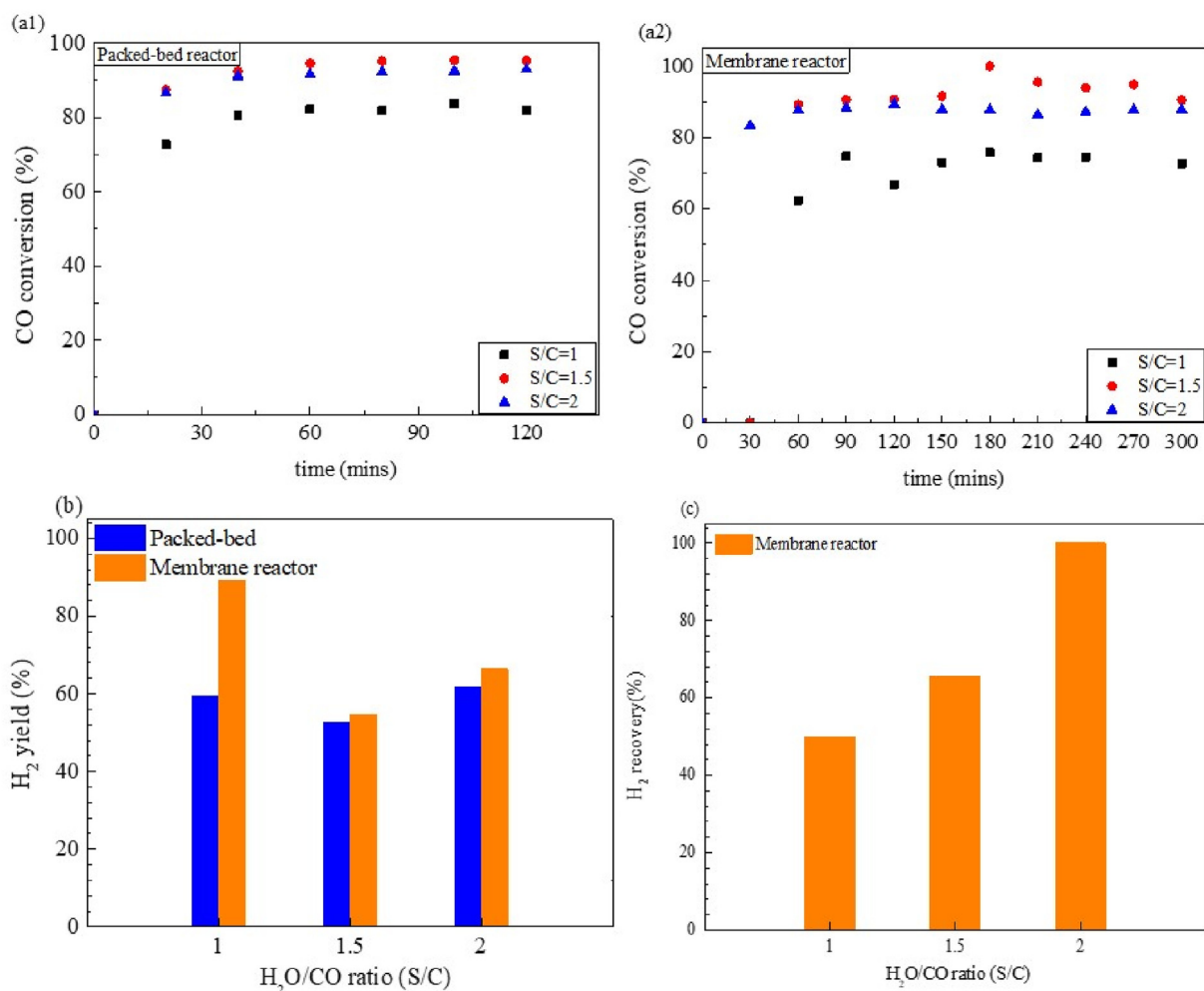


**Fig. 9** – LT-WGS activities of packed-bed reactor and C membrane reactor mode of Cu/Zn/SBA-16 catalyst as a function of H<sub>2</sub>O/CO ratio: (a) CO conversion; (b) H<sub>2</sub> yield and (c) H<sub>2</sub> recovery (reaction conditions: reaction temperature of 300 °C; space velocity of 2500 h<sup>-1</sup>).

consistent with the expected results. However, in past research [57,70], scholars have suggested that when the steam content is high, it may be adsorbed on the catalyst surface active sites and cause competitive adsorption with CO, resulting in the decline of CO conversion, which is the same finding as described above in the packed bed.

#### Improving CO conversion by coating with a hydrophobic protective layer

To effectively enhance the CO conversion of the C membrane reactor, the C membrane surface was modified by coating with a hydrophobic layer, trichlorododecylsilane, and the reaction was carried out at a steam ratio of 2. The results are shown in Fig. 10, which represent the CO conversion obtained from the unmodified and Si-modified membrane reactors. It was found that the Si-modified C membrane reached a steady-state after 60 min and had a higher CO conversion of up to

100% during 300 min of testing. Compared to the unmodified C membrane, the CO conversion rate of the Si-modified membrane (Si/C membrane) exhibited a high performance even under a high steam ratio, which indicated that the hydrophobicity of the CMS membranes was enhanced after coating a trichlorododecylsilane layer on the surface. Table 3 shows the contact angles of the CMS membranes modified with or without a hydrophobic protective layer. As Table 3 shows, after surface modification, the hydrophobicity of the membrane was remarkably improved; further, the membrane maintained a very high hydrophobic performance after 5–6 h of the WGS reaction. FE-SEM images of the Si/C CMS membranes and the composition of each element in the modified membrane are shown in Fig. S5 and Table S1, which show that the silane thin film is approximately 0.31% of the total composition. In addition, it can be observed in Fig. S5 (c4) that the silane layer is uniformly dispersed in the membrane structure.

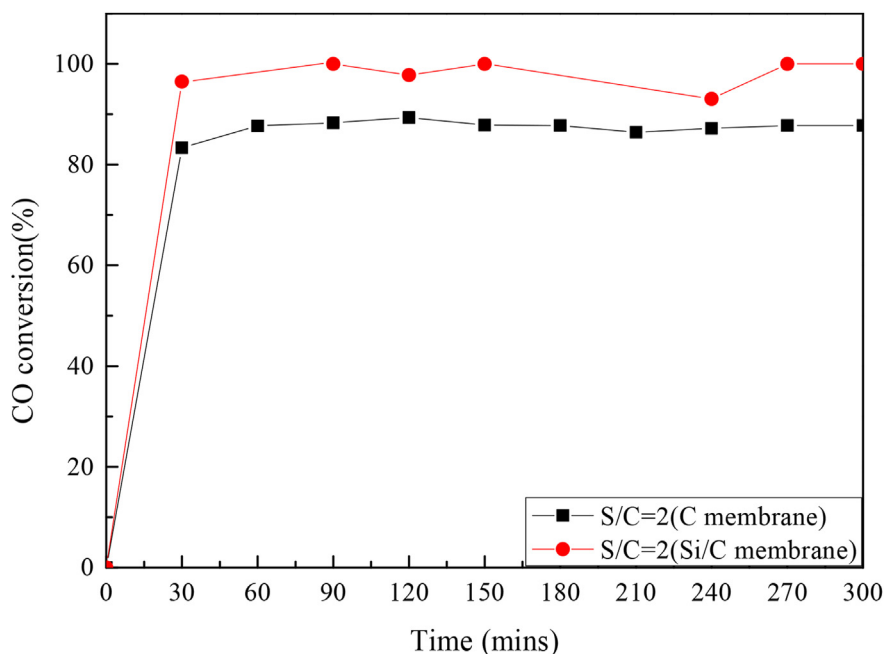


**Fig. 10 – The long-term stability of LT-WGS reaction of membrane reactor mode with and without coating a trichlorododecylsilane hydrophobic protective layer.**

**Table 3 – Contact angles of the non-modified and modified membranes and the modified-membrane after the reaction.**

Membrane code	Non-modified membrane	Modified membrane	Modified membrane after reaction
Contact angle (°)	83.89 ± 2.54	106.43 ± 0.76	104.56 ± 0.69

## Conclusion

In this study, a C membrane was employed as a membrane reactor and applied in the WGS reaction as a high-performance membrane with high thermal stability, environmental tolerance, and ideal H<sub>2</sub>/CO<sub>2</sub> permselectivity. The as-prepared CMS membrane exhibited a maximum selectivity of 185.64 for 50/50 binary gas composed of H<sub>2</sub> and CO<sub>2</sub> and presented an ideal H<sub>2</sub> permeability of  $9.7 \times 10^{-9}$  mol m<sup>-2</sup> s<sup>-1</sup> Pa<sup>-1</sup> when operated under 3 bars.

Cu/Zn/SBA-16 was synthesized as a WGS catalyst. At a 300 °C reaction temperature, 2500 h<sup>-1</sup> GHSV, and S/C = 1.5, the CO conversion efficiency of the C membrane reactor could reach 99% and the recovery of H<sub>2</sub> was approximately 76%. However, as the S/C increased to 2, the H<sub>2</sub> recovery increased to 99%, and the CO conversion slightly decreased to 89% because of the water vapor adsorbed on the active site.

After hydrophobic modification, the modified CMS membrane showed recovered CO conversion of over 99% with S/C = 2. In summary, a tubular CMS membrane reactor was successfully fabricated and showed promising potential for extensive development.

## Declaration of competing interest

The authors declare that we have no conflict of interest with other people or organizations. There is no professional or other personal interest of any nature or kind in any product.

## Acknowledgement

The authors gratefully acknowledge the financial support provided by the Ministry of Science and Technology (MOST), Taiwan. (MOST 103-2221-E-040-001-MY3)

## Appendix A. Supplementary data

Supplementary data to this article can be found online at <https://doi.org/10.1016/j.ijhydene.2022.11.199>.

## REFERENCES

- [1] Bracht M, Alderliesten PT, Kloster R, Pruscek R, Haupt G, Xue E, et al. Water gas shift membrane reactor for CO<sub>2</sub> control in IGCC systems: techno-economic feasibility study. *Energy Convers Manag* 1997;38:S159–64.
- [2] Ahmed U, Zahid U, Jeong YS, Lee C-J, Han C. IGCC process intensification for simultaneous power generation and CO<sub>2</sub> capture. *Chem Eng Process: Process Intensif* 2016;101:72–86.
- [3] Carbo MC, Boon J, Jansen D, van Dijk HAJ, Dijkstra JW, van den Brink RW, et al. Steam demand reduction of water–gas

- shift reaction in IGCC power plants with pre-combustion CO<sub>2</sub> capture. *Int J Greenh Gas Control* 2009;3:712–9.
- [4] Iulianelli A, Pirola C, Comazzi A, Galli F, Manenti F, Basile A. 1 - water gas shift membrane reactors. *Membrane Reactors for Energy Applications and Basic Chemical Production*: Woodhead Publishing 2015:3–29.
- [5] Chein RY, Chen YC, Chung JN. Sweep gas flow effect on membrane reactor performance for hydrogen production from high-temperature water-gas shift reaction. *J Membr Sci* 2015;475:193–203.
- [6] Galuszka J, Giddings T, Iaquaniello G. Membrane assisted WGSR – experimental study and reactor modeling. *Chem Eng J* 2012;213:363–70.
- [7] Querino PS, Bispo JRC, Rangel MdC. The effect of cerium on the properties of Pt/ZrO<sub>2</sub> catalysts in the WGSR. *Catal Today* 2005;107–108:920–5.
- [8] Sá S, Sousa JM, Mendes A. Steam reforming of methanol over a CuO/ZnO/Al<sub>2</sub>O<sub>3</sub> catalyst part II: a carbon membrane reactor. *Chem Eng Sci* 2011;66:5523–30.
- [9] Sagata K, Kaneda Y, Yamaura H, Kobayashi S, Yahiro H. Influence of coexisting Al<sub>2</sub>O<sub>3</sub> on the activity of copper catalyst for water–gas-shift reaction. *Int J Hydrogen Energy* 2014;39:20639–45.
- [10] Li L, Song L, Wang H, Chen C, She Y, Zhan Y, et al. Water-gas shift reaction over CuO/CeO<sub>2</sub> catalysts: effect of CeO<sub>2</sub> supports previously prepared by precipitation with different precipitants. *Int J Hydrogen Energy* 2011;36:8839–49.
- [11] Shishido T, Nishimura S, Yoshinaga Y, Ebitani K, Teramura K, Tanaka T. High sustainability of Cu–Al–Ox catalysts against daily start-up and shut-down (DSS)-like operation in the water–gas shift reaction. *Catal Commun* 2009;10:1057–61.
- [12] Yahiro H, Nakaya K, Yamamoto T, Saiki K, Yamaura H. Effect of calcination temperature on the catalytic activity of copper supported on  $\gamma$ -alumina for the water-gas-shift reaction. *Catal Commun* 2006;7:228–31.
- [13] Utaka T, Sekizawa K, Eguchi K. CO removal by oxygen-assisted water gas shift reaction over supported Cu catalysts. *Appl Catal Gen* 2000;194–195:21–6.
- [14] Sagata K, Imazu N, Yahiro H. Study on factors controlling catalytic activity for low-temperature water–gas-shift reaction on Cu-based catalysts. *Catal Today* 2013;201:145–50.
- [15] Kowalik P, Konkol M, Antoniak K, Próchniak W, Wiercioch P. The effect of the precursor ageing on properties of the Cu/ZnO/Al<sub>2</sub>O<sub>3</sub> catalyst for low temperature water–gas shift (LT-WGS). *J Mol Catal Chem* 2014;392:127–33.
- [16] Á Szegedi, Popova M, Lázár K, Klébert S, Drotár E. Impact of silica structure of copper and iron-containing SBA-15 and SBA-16 materials on toluene oxidation. *Microporous Mesoporous Mater* 2013;177:97–104.
- [17] Azizi SN, Ghasemi S, Yazdani-Sheldarrei H. Synthesis of mesoporous silica (SBA-16) nanoparticles using silica extracted from stem cane ash and its application in electrocatalytic oxidation of methanol. *Int J Hydrogen Energy* 2013;38:12774–85.
- [18] Gobin OC. SBA-16 materials synthesis, diffusion and sorption properties. 2006.
- [19] Lin C-W. Synthesis, characterization and hydrothermal stability of titanosilicate SBA-16 and Zr-containing SBA-15 nanoporous materials. 2005.
- [20] Zhuravlev LT. The surface chemistry of amorphous silica. *Zhuravlev model. Colloids and Surfaces A: Physicochemical and Engineering Aspects* 2000;173:1–38.
- [21] Criscuoli A, Basile A, Drioli E, Loiacono O. An economic feasibility study for water gas shift membrane reactor. *J Membr Sci* 2001;181:21–7.
- [22] Lee D, Oyama ST. Gas permeation characteristics of a hydrogen selective supported silica membrane. *J Membr Sci* 2002;210:291–306.
- [23] Yang X, Wang S, He Y. Review of catalytic reforming for hydrogen production in a membrane-assisted fluidized bed reactor. *Renew Sustain Energy Rev* 2022;154:111832.
- [24] Adhikari S, Fernando S. Hydrogen membrane separation techniques. *Ind Eng Chem Res* 2006;45:875–81.
- [25] Rahimpour MR, Samimi F, Babapoor A, Tohidian T, Mohebi S. Palladium membranes applications in reaction systems for hydrogen separation and purification: a review. *Chem Eng Process: Process Intensif* 2017;121:24–49.
- [26] Song IK, Lee WY, Kim JJ. Application of heteropoly acid catalyst in an inert polymer membrane catalytic reactor in ethanol dehydration. *Catal Lett* 1991;9:339–45.
- [27] Ernst B, Haag S, Burgard M. Permselectivity of a nickel/ceramic composite membrane at elevated temperatures: a new prospect in hydrogen separation? *J Membr Sci* 2007;288:208–17.
- [28] Bi Y, Xu H, Li W, Goldbach A. Water–gas shift reaction in a Pd membrane reactor over Pt/Ce<sub>0.6</sub>Zr<sub>0.4</sub>O<sub>2</sub> catalyst. *Int J Hydrogen Energy* 2009;34:2965–71.
- [29] Zhang K, Way JD. Palladium-copper membranes for hydrogen separation. *Separ Purif Technol* 2017;186:39–44.
- [30] Maneerung T, Hidajat K, Kawi S. Triple-layer catalytic hollow fiber membrane reactor for hydrogen production. *J Membr Sci* 2016;514:1–14.
- [31] Zuo C, Lee TH, Dorris SE, Balachandran U, Liu M. Composite Ni–Ba(Zr<sub>0.1</sub>Ce<sub>0.7</sub>Y<sub>0.2</sub>)O<sub>3</sub> membrane for hydrogen separation. *J Power Sources* 2006;159:1291–5.
- [32] García-García FR, Rahman MA, González-Jiménez ID, Li K. Catalytic hollow fibre membrane micro-reactor: high purity H<sub>2</sub> production by WGS reaction. *Catal Today* 2011;171:281–9.
- [33] Battersby SE, Miller D, Zed M, Patch J, Rudolph V, Duke MC, et al. Silica membrane reactors for hydrogen processing. *Adv Appl Ceram* 2007;106:29–34.
- [34] Sá S, Silva H, Sousa JM, Mendes A. Hydrogen production by methanol steam reforming in a membrane reactor: palladium vs carbon molecular sieve membranes. *J Membr Sci* 2009;339:160–70.
- [35] Peng L, Rao Y, Luo L, Chen CA. The poisoning of Pd–Y alloy membranes by carbon monoxide. *J Alloys Compd* 2009;486:74–7.
- [36] Gabitto JF, Tsouris C. Sulfur poisoning of metal membranes for hydrogen separation. *International Review of Chemical Engineering* 2009;1:394–411.
- [37] Scholes CA, Kentish SE, Stevens GW. Effects of minor components in carbon dioxide capture using polymeric gas separation membranes. *Separ Purif Rev* 2009;38:1–44.
- [38] Basile A, Criscuoli A, Santella F, Drioli E. Membrane reactor for water gas shift reaction. *Gas Separ Purif* 1996;10:243–54.
- [39] Tseng H-H, Wang C-T, Zhuang G-L, Uchytel P, Reznickova J, Setnickova K. Enhanced H<sub>2</sub>/CH<sub>4</sub> and H<sub>2</sub>/CO<sub>2</sub> separation by carbon molecular sieve membrane coated on titania modified alumina support: effects of TiO<sub>2</sub> intermediate layer preparation variables on interfacial adhesion. *J Membr Sci* 2016;510:391–404.
- [40] Jiao W, Ban Y, Shi Z, Jiang X, Li Y, Yang W. Gas separation performance of supported carbon molecular sieve membranes based on soluble polybenzimidazole. *J Membr Sci* 2017;533:1–10.
- [41] Hamm JBS, Muniz AR, Pollo LD, Marcilio NR, Tessaro IC. Experimental and computational analysis of carbon molecular sieve membrane formation upon polyetherimide pyrolysis. *Carbon* 2017;119:21–9.
- [42] Briceño K, Iulianelli A, Montané D, Garcia-Valls R, Basile A. Carbon molecular sieve membranes supported on non-

- modified ceramic tubes for hydrogen separation in membrane reactors. *Int J Hydrogen Energy* 2012;37:13536–44.
- [43] Hirota Y, Ishikado A, Uchida Y, Egashira Y, Nishiyama N. Pore size control of microporous carbon membranes by post-synthesis activation and their use in a membrane reactor for dehydrogenation of methylcyclohexane. *J Membr Sci* 2013;440:134–9.
- [44] Tennison SR, Arnott K, Richter H. Carbon ceramic composite membranes for catalytic membrane reactor applications. *Kinet Catal* 2007;48:864–76.
- [45] Ngamou PHT, Ivanova ME, Guillon O, Meulenber WA. High-performance carbon molecular sieve membranes for hydrogen purification and pervaporation dehydration of organic solvents. *J Mater Chem* 2019;7:7082–91.
- [46] Zhang B, Wang D, Zhou J, Wu Y, Zhao D, Wang T, et al. Process intensification of the hydrogen production reaction using a carbon membrane reactor: kinetics analysis. *Energy Technol* 2017;5:1990–7.
- [47] Fu S, Sanders ES, Kulkarni S, Chu Y-H, Wenz GB, Koros WJ. The significance of entropic selectivity in carbon molecular sieve membranes derived from 6FDA/DETDA:DABA(3:2) polyimide. *J Membr Sci* 2017;539:329–43.
- [48] Rungta M, Wenz GB, Zhang C, Xu L, Qiu W, Adams JS, et al. Carbon molecular sieve structure development and membrane performance relationships. *Carbon* 2017;115:237–48.
- [49] Wey M-Y, Chen H-H, Lin Y-T, Tseng H-H. Thin carbon hollow fiber membrane with Knudsen diffusion for hydrogen/alkane separation: effects of hollow fiber module design and gas flow mode. *Int J Hydrogen Energy* 2020;45:7290–302.
- [50] Battersby S, Smart S, Ladewig B, Liu S, Duke MC, Rudolph V, et al. Hydrothermal stability of cobalt silica membranes in a water gas shift membrane reactor. *Separ Purif Technol* 2009;66:299–305.
- [51] Jones CW, Koros WJ. Carbon composite membranes: a solution to adverse humidity effects. *Ind Eng Chem Res* 1995;34:164–7.
- [52] Chen J, You H, Xu L, Li T, Jiang X, Li CM. Facile synthesis of a two-tier hierarchical structured superhydrophobic-superoleophilic melamine sponge for rapid and efficient oil/water separation. *J Colloid Interface Sci* 2017;506:659–68.
- [53] Stevens WJJ, Lebeau K, Mertens M, Van Tendeloo G, Cool P, Vansant EF. Investigation of the morphology of the mesoporous SBA-16 and SBA-15 materials. *J Phys Chem B* 2006;110:9183–7.
- [54] Van Der Voort P, Benjelloun M, Vansant EF. Rationalization of the synthesis of SBA-16: controlling the micro- and mesoporosity. *J Phys Chem B* 2002;106:9027–32.
- [55] Li J-Y, Tseng H-H, Wey M-Y. Tuning thermal expansion behavior and surface roughness of tubular  $\text{Al}_2\text{O}_3$  substrates for fabricating high-performance carbon molecular sieving membranes for  $\text{H}_2$  separation. *Int J Hydrogen Energy* 2019;44:24746–58.
- [56] Li J-Y, Cheng P-Y, Lin M-D, Wey M-Y, Tseng H-H. Uniformity control and ultra-micropore development of tubular carbon membrane for light gas separation. *AIChE J* 2020;66:e16226.
- [57] Fujita S-i, Kanamori Y, Satriyo AM, Takezawa N. Methanol synthesis from  $\text{CO}_2$  over Cu/ZnO catalysts prepared from various coprecipitated precursors. *Catal Today* 1998;45:241–4.
- [58] Zhang H, Wang J, Liu T, Zhang M, Hao L, Phouththavong T, et al. Cu-Zn oxides nanoparticles supported on SBA-15 zeolite as a novel adsorbent for simultaneous removal of  $\text{H}_2\text{S}$  and  $\text{H}_2\text{O}$  in natural gas. *Chem Eng J* 2021;426:131286.
- [59] Nakamura J, Nakamura I, Uchijima T, Watanabe T, Fujitani T. Model studies of methanol synthesis on copper catalysts. In: Hightower JW, Nicholas Delgass W, Iglesia E, Bell AT, editors. *Studies in surface science and catalysis*. Elsevier; 1996. p. 1389–99.
- [60] Budiman A, Ridwan M, Kim SM, Choi J-W, Yoon CW, Ha J-M, et al. Design and preparation of high-surface-area Cu/ZnO/ $\text{Al}_2\text{O}_3$  catalysts using a modified co-precipitation method for the water-gas shift reaction. *Appl Catal, A* 2013;462:220–6.
- [61] Jain R, Maric R. Synthesis of nano-Pt onto ceria support as catalyst for water-gas shift reaction by Reactive Spray Deposition Technology. *Appl Catal Gen* 2014;475:461–8.
- [62] Ammal SC, Heyden A. Origin of the unique activity of Pt/TiO<sub>2</sub> catalysts for the water-gas shift reaction. *J Catal* 2013;306:78–90.
- [63] Liu P. Chapter 9 - synergistic effect of metal/oxide catalysts in the water-gas shift reactions: a theory-guided rational design of better catalysts A2 - suib. In: Steven L. New and future developments in catalysis. Amsterdam: Elsevier; 2013. p. 213–41.
- [64] Atake I, Nishida K, Li D, Shishido T, Oumi Y, Sano T, et al. Catalytic behavior of ternary Cu/ZnO/ $\text{Al}_2\text{O}_3$  systems prepared by homogeneous precipitation in water-gas shift reaction. *J Mol Catal Chem* 2007;275:130–8.
- [65] Koryabkina NA, Phatak AA, Ruettinger WF, Farrauto RJ, Ribeiro FH. Determination of kinetic parameters for the water-gas shift reaction on copper catalysts under realistic conditions for fuel cell applications. *J Catal* 2003;217:233–9.
- [66] Jeong Y, Kim I, Kang JY, Yan N, Jeong H, Park JK, et al. Effect of the aging time of the precipitate on the activity of Cu/ZnO catalysts for alcohol-assisted low temperature methanol synthesis. *J Mol Catal Chem* 2016;418-419:168–74.
- [67] Sing KSW. Reporting physisorption data for gas/solid systems with special reference to the determination of surface area and porosity (Recommendations 1984). *Pure Appl Chem* 1985;57:603–19.
- [68] Dong X, Wang H, Rui Z, Lin YS. Tubular dual-layer MFI zeolite membrane reactor for hydrogen production via the WGS reaction: experimental and modeling studies. *Chem Eng J* 2015;268:219–29.
- [69] Oluku IJ. Hydrogen production by water gas shift reaction following dry reforming of biogas methane in membrane and packed bed tubular reactors: faculty of graduate studies and research. University of Regina; 2013.
- [70] Liu B, Zong Q, Du X, Zhang Z, Xiao T, AlMegren H. Novel sour water gas shift catalyst (SWGS) for lean steam to gas ratio applications. *Fuel Process Technol* 2015;134:65–72.